9402 *Inorg. Chem.* **2009**, *48*, 9402–9408
DOI: 10.1021/ic901295d

Inorganic Chemistry
Article

Chromium Acetylide Complex Based Ferrimagnet and Weak Ferromagnet

Junichi Nishijo, Ken Judai, Shigenori Numao, and Nobuyuki Nishi*

Department of Materials Molecular Science, Institute for Molecular Science, 38 Nishigo-Naka, Myodaiji, Okazaki 444-8585, Japan

Received July 6, 2009

The crystal structures and magnetic properties of new molecule-based magnets, [CrCyclam(C≡C−3-thiophene)$_2$]-[Ni(mdt)$_2$] (**1**) and [CrCyclam(C≡C−Ph)$_2$][Ni(mdt)$_2$](H$_2$O) (**2**) (Cyclam = 1,4,8,11-tetraazacyclotetradecane, mdt = 1,3-dithiole-4,5-dithiolate), are reported. The crystal structures of both compounds are characterized by ferrimagnetic chains of alternately stacked [CrCyclam(C≡C−R)]$^+$ cations and [Ni(mdt)$_2$]$^-$ anions with intrachain exchange interactions of $2J = -6.1$ K in **1** and -5.7 K in **2** ($H = -2J\sum_i S_i \cdot S_{i+1}$). The material **1** exhibits ferrimagnetic transition at 2.3 K owing to weak interchain antiferromagnetic interactions between cations and anions. In the case of **2**, cations in adjacent ferrimagnetic chains are bridged by a water molecule, resulting in an interchain antiferromagnetic coupling. Despite a centrosymmetry of a whole crystal of **2**, one bridging water molecule occupies only one of the two centrosymmetric sites and breaks a local centrosymmetry between adjacent cations. The interchain antiferromagnetic interaction and Dzyaloshinsky−Moriya interaction originated from the local symmetry breakdown of **2** bring a weak-ferromagnetic transition at 3.7 K with a coercive force of less than 0.8 mT, followed by the second magnetic phase transition at 2.9 K. Below this temperature, the coercive force rapidly increases from 1 to 11.8 mT as the temperature decreases from 2.9 to 1.8 K, while the remanent magnetization monotonically increases from 0.008 μ_B at 3.6 K to 0.12 μ_B at 1.8 K.

Introduction

In the past few decades, there has been an extensive effort to investigate the area of molecule-based magnetic materials, and developing new classes of magnetic materials brings a lot of new findings such as organic ferromagnets,[1,2] single-molecule magnets,[3,4] single-chain magnets,[5−7] magnetically controlled conductivities,[8−12] chiral magnets,[13−18] and so forth. Among the large number of building blocks of

*To whom correspondence should be addressed. Tel.: +81-564-55-7350. Fax: +81-564-54-2254. E-mail: nishi@ims.ac.jp.

(1) Kinoshita, M.; Turek, P.; Tamura, M.; Nozawa, K.; Shiomi, D.; Nakazawa, Y.; Ishikawa, M.; Takahashi, M.; Awaga, K.; Inabe, T.; Maruyama, Y. *Chem. Lett.* **1991**, 1225–1228.
(2) Nakatsuji, S.; Anzai, H. *J. Mater. Chem.* **1997**, *7*, 2161−2174 and references therein.
(3) Sessoli, R.; Gatteschi, D.; Caneschi, A.; Noval, M. A. *Nature* **1993**, *365*, 141–143.
(4) Sessoli, R.; Tsai, H. L.; Schake, A. R.; Wang, S.; Vincent, J. B.; Folting, K.; Gatteschi, D.; Christou, G.; Hendrickson, D. N. *J. Am. Chem. Soc.* **1993**, *115*, 1804–1816.
(5) Caneschi, A.; Gatteschi, D.; Lalioti, N.; Sangregorio, C.; Sessoli, R.; Venturi, G.; Vindigni, A.; Rettori, A.; Pini, M. G.; Novak, M. A. *Angew. Chem., Int. Ed.* **2001**, *40*, 1760–1763.
(6) Clerac, R.; Miyasaka, H.; Yamashita, M.; Coulon, C. *J. Am. Chem. Soc.* **2002**, *124*, 12837–12844.
(7) Bogani, L.; Vindigni, A.; Sessoli, R.; Gatteschi, D. *J. Mater. Chem.* **2008**, *18*, 4750−4758 and references therein.
(8) Hanasaki, N.; Tajima, H.; Matsuda, M.; Naito, T.; Inabe, T. *Phys. Rev. B* **2000**, *62*, 5839–5842.
(9) Uji, S.; Shinagawa, H.; Terashima, T.; Yakabe, T.; Terai, Y.; Tokumoto, M.; Kobayashi, A.; Tanaka, H.; Kobayashi, H. *Nature* **2001**, *410*, 908–910.
(10) Okabe, K.; Yamaura, J.-I.; Miyazaki, A.; Enoki, T. *J. Phys. Soc. Jpn.* **2005**, *74*, 1508–1520.
(11) Nishijo, J.; Miyazaki, A.; Enoki, T.; Watanabe, R.; Kuwatani, Y.; Iyoda, M. *Inorg. Chem.* **2005**, *44*, 2493–2506.
(12) Miyazaki, A.; Yamazaki, H.; Aimatsu, M.; Enoki, T.; Watanabe, R.; Ogura, E.; Kuwatani, Y.; Iyoda, M. *Inorg. Chem.* **2007**, *46*, 3353–3366.
(13) Kumagai, H.; Inoue, K. *Angew. Chem., Int. Ed.* **1999**, *38*, 1601–1603.
(14) Inoue, K.; Imai, H.; Ghalsasi, P. S.; Kikuchi, K.; Ohba, M.; Okawa, H.; Yakhmi, J. V. *Angew. Chem., Int. Ed.* **2001**, *40*, 4242–4245.
(15) Minguet, M.; Luneau, D.; Lhotel, E.; Villar, V.; Paulsen, C.; Amabilino, D. B.; Veciana, J. *Angew. Chem., Int. Ed.* **2002**, *41*, 586–589.
(16) Coronado, E.; Gómez-García, C. J.; Nuez, A.; Romero, F. M. *Chem. Mater.* **2006**, *18*, 2670–2681.
(17) Numata, Y.; Inoue, K.; Baranov, N.; Kurmoo, M.; Kikuchi, K. *J. Am. Chem. Soc.* **2007**, *129*, 9902–9909.
(18) Clemente-León, M.; Coronado, E.; Dias, J. C.; Soriano-Portillo, A.; Willett, R. D. *Inorg. Chem.* **2008**, *47*, 6458–6463.
(19) Ferlay, S.; Mallah, T.; Ouahes, R.; Veillet, P.; Verdaguer, M. *Nature* **1995**, *378*, 701–703.
(20) Sato, O.; Iyoda, T.; Fujishima, A.; Hashimoto, K. *Science* **1996**, *272*, 704–705.
(21) Manriquez, J. M.; Yee, G. T.; McLean, R. S.; Epstein, A. J.; Miller, J. S. *Science* **1991**, *252*, 1415–1417.
(22) Podgajny, R.; Pinkowicz, D.; Korzeniak, T.; Nitek, W.; Rams, M.; Sieklucka, B. *Inorg. Chem.* **2007**, *46*, 10416–10425.
(23) Johnson, M. T.; Arif, A. M.; Miller, J. S. *Eur. J. Inorg. Chem.* **2000**, 1781–1787.

Published on Web 09/11/2009

molecule-based magnetic materials, transition metal complexes with a coordinating cyano group have been a major subject of intensive study.[19−25] Nevertheless, in contrast to the fact that there are a number of reports on $M^{n+}(N{\equiv}C-R)_m$-type molecule-based magnets, relatively few studies have been reported regarding their isoelectronic carbon analogues, the transition metal acetylides $M^{n+}(C{\equiv}C-R)_m{}^{m-}$, because most of the transition metal acetylides are easily decomposed under the existence of oxygen or water.[26−28] Recently, efforts to design new transition metal acetylides have led to the development of air- and water-stable paramagnetic acetylides,[29−37] where multidentate ligands protect the complexes from decomposition. These stable transition metal acetylides show interesting optical and electrochemical properties and strong intramolecular spin−spin interactions and have considerable promise as molecule-based bulk magnets. However, to our knowledge, no attempt has succeeded in constructing the molecule-based magnets by using transition metal acetylides.

In this paper, we report on the preparations, the crystal structures, and the magnetic properties of the transition metal acetylide based magnets. Among the several kinds of stable transition metal acetylides, we employed the chromium complex $[CrCyclam(C{\equiv}C-R)_2]^+$ (R = 3-thiophene, Ph; Cyclam = 1,4,8,11-tetraazacyclotetradecane) as a magnetic cation because its large magnetic moment ($S = 3/2$) is suitable for producing a strong intermolecular exchange interaction and bringing a magnetic transition. Meanwhile, the nickel dithiolate $[Ni(mdt)_2]^-$ (mdt = 1,3-dithiole-4,5-dithiolate) was used as a paramagnetic counteranion. Transition metal dithiolate anions are known to have a large π-orbital perpendicular to the molecular plane, which enhances intermolecular orbital overlaps, resulting in the strong intermolecular exchange interaction.[38] The obtained new materials, $[CrCyclam(C{\equiv}C-3\text{-thiophene})_2][Ni(mdt)_2]$ (**1**) and $[CrCyclam(C{\equiv}C-Ph)_2][Ni(mdt)_2](H_2O)$ (**2**), are, as far as the authors know, the first examples of a ferrimagnet and weak-ferromagnet containing a transition metal acetylide.

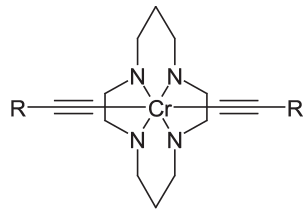

$[CrCyclam(C{\equiv}C\text{-}R)_2]^+$

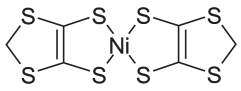

$[Ni(mdt)_2]^-$

Experimental Section

Synthesis. $[CrCyclam(C{\equiv}C-Ph)_2]OTf$ (OTf = trifluoromethanesulfonate) and $(C_4H_9)_4N[Ni(mdt)_2]$ were prepared according to literature methods.[35,39−41] $[CrCyclam(C{\equiv}C\text{-}3\text{-thiophene})_2]OTf\cdot H_2O$ was synthesized by the same method where 3-ethynylthiophene was used rather than phenylacetylene (yield: 55%, anal. calcd for $C_{23}H_{32}Cr_1F_3N_4O_4S_3$: C, 43.59; H, 5.09; N, 8.84; S, 15.18%, Found: C, 43.22; H, 5.07; N, 8.69; S, 14.99%). Thin plate crystals of **1** and small needle crystals of **2** were precipitated by mixing a solution of $[CrCyclam(C{\equiv}C-3\text{-thiophene})_2]OTf\cdot H_2O$ or $[CrCyclam(C{\equiv}C-Ph)_2]OTf$ (40 mg) in 1,2-dichloroethane (30 mL) with a solution of $(C_4H_9)_4N[Ni(mdt)_2]$ (40 mg) in chlorobenzene (25 mL) within a day, where solvents were used without any purification. In the case of **2**, the yield can be increased by adding a small portion of water, while the crystal size becomes smaller. Typical crystal sizes are ca. $0.15 \times 0.15 \times 0.005$ mm^3 for **1** and $0.4 \times 0.04 \times 0.005$ mm^3 for **2**.

Single-Crystal X-ray Diffraction. X-ray diffraction measurements were carried out on a Rigaku AFC-7R four-circle diffractometer (fine focus type) with a Mercury CCD area detector at 293 K, using Mo Kα radiation ($\lambda = 0.7107$ Å). The structures were solved using direct methods (SIR2004)[42] then refined with a full-matrix least-squares method (SHELXL-97).[43] An absorption correction based on Ψ-scan was introduced. All nonhydrogen atoms were refined anisotropically, while hydrogen atoms were placed in their calculated positions and refined using the riding model. Crystallographic data are summarized in Table 1. Full bond lengths and bond angles, atomic coordinates, and complete crystal structure results are provided as Supporting Information.

Magnetic Susceptibility Measurements. DC and AC magnetic susceptibilities were measured using a Quantum-Design MPMS-XL7 SQUID magnetometer for randomly oriented single crystals encapsulated in aluminum capsules. Diamagnetic

(24) Miyasaka, H.; Madanbashi, T.; Sugimoto, K.; Nakazawa, Y.; Wernsdorfer, W.; Sugiura, K.; Yamashita, M.; Coulon, C.; Clérac, R. *Chem.—Eur. J.* **2006**, *12*, 7028–7040.
(25) Hünig, S.; Erk, P. *Adv. Mater.* **1991**, *3*, 225–236.
(26) Nast, R. *Coord. Chem. Rev.* **1982**, *47*, 89–124.
(27) Shaw-Taberlet, J. A.; Sinbandhit, S.; Roisnel, T.; Hamon, J.-R.; Lapinte, C. *Organomet.* **2006**, *25*, 5311–5325.
(28) Berben, L. A.; Long, J. R. *Inorg. Chem.* **2005**, *44*, 8459−8468 and references therein.
(29) Krivykh, V. V.; Eremenko, I. L.; Veghini, D.; Petrunenko, I. A.; Pountney, D. L.; Unseld, D.; Berke, H. *J. Organomet. Chem.* **1996**, *511*, 111–114.
(30) Unseld, D.; Krivykh, V. V.; Heinze, K.; Wild, F.; Artus, G.; Schmalle, H.; Berke, H. *Organomet.* **1999**, *18*, 1525–1541.
(31) Kheradmandan, S.; Fox, T.; Schmalle, H. W.; Venkatesan, K.; Berke, H. *Eur. J. Inorg. Chem.* **2004**, 3544–3554.
(32) Venkatesan, K.; Fox, T.; Schmalle, H. W.; Berke, H. *Organomet.* **2005**, *24*, 2834–3847.
(33) Klein, A.; Lavastre, O.; Fiedler, J. *Organomet.* **2006**, *25*, 635–643.
(34) Rupp, R.; Huttner, G.; Lang, H.; Heinze, K.; Büchner, M.; Hovestreydt, E. R. *Eur. J. Inorg. Chem.* **2000**, 1953–1959.
(35) Grisenti, D. L.; Thomas, W. W.; Turlington, C. R.; Newsom, M. D.; Priedemann, C. J.; VanDerveer, D. G.; Wagenknecht, P. S. *Inorg. Chem.* **2008**, *47*, 11452–11454.
(36) Hamon, P.; Justaud, F.; Cador, O.; Hapiot, P.; Rigaut, S.; Toupet, L.; Ouahab, L.; Stueger, H.; Hamon, J.-R.; Lapinte, C. *J. Am. Chem. Soc.* **2008**, *130*, 17372–17383.
(37) Berben, L. A.; Long, J. R. *J. Am. Chem. Soc.* **2002**, *124*, 11588–11589.
(38) Robertson, N.; Cronin, L. *Coord. Chem. Rev.* **2002**, *227*, 93–127.
(39) Wright-Garcia, K.; Basinger, J.; Williams, S.; Hu, C.; Wagenknecht, P. S. *Inorg. Chem.* **2003**, *42*, 4885–4890.
(40) Bakac, A.; Espenson, J. H. *Inorg. Chem.* **1992**, *31*, 1108–1110.
(41) Veldhuizen, Y. S. J.; Veldman, N.; Spek, A. L.; Cassoux, P.; Carlier, R.; Mulder, M. J. J.; Haasnoot, J. G.; Reedijk, J. *J. Chem. Soc., Dalton Trans.* **1998**, 2989–2993.
(42) Burla, M. C.; Caliandro, R.; Camalli, M.; Carrozzini, B.; Cascarano, G. L.; De Caro, L.; Giacovazzo, C.; Polidori, G.; Spagna, R. *J. Appl. Crystallogr.* **2005**, *38*, 381–388.
(43) Sheldrick, G. M. *Acta Crystallogr., Sect. A* **2008**, *64*, 112–122.

Table 1. Crystal Data and Structure Refinement for **1** and **2**

	1	**2**
mol formula	$C_{28}H_{34}Cr_1N_4Ni_1S_{10}$	$C_{32}H_{40}Cr_1N_4Ni_1O_1S_8$
fw	857.95	863.91
temp/K	293(2)	293(2)
radiation, λ/Å	0.71073	0.71073
cryst syst	monoclinic	triclinic
space group	$P21/c$ (No. 14)	$P\bar{1}$ (No. 2)
a/Å	12.217(2)	8.3836(5)
b/Å	12.4180(18)	11.1713(5)
c/Å	13.358(2)	12.4272(7)
α/deg	90	63.993(10)
β/deg	116.752(4)	72.577(12)
γ/deg	90	70.708(12)
V/Å^3	1809.6(5)	970.76(9)
Z	2	1
d_{calcd}/g cm^{-3}	1.574	1.478
no. of reflns collected	4904	4676
no. of ind reflns	4697	4676
$I > 2\sigma I$	3287	2903
final R1[a], wR2[b]	0.0552, 0.1543	0.0650, 0.1932

[a] $R = \sum||F_o| - |F_c||/\sum|F_o|$. [b] $wR2 = \{\sum[w(F_o^2 - F_c^2)^2]/\sum[w(F_o^2)^2]\}^{1/2}$.

corrections were estimated from Pascal's constants as -443×10^{-6} (**1**) and -460×10^{-6} (**2**) cm^{3}mol^{-1}.

Results and Discussion

Crystal Structure of 1. ORTEP[44] drawings of the molecular structure with the atomic numbering scheme and selected bond distances and bond angles for **1** are shown in Figure 1a and Table 2, respectively. The asymmetric unit of **1** consists of half a cation and half an anion, where cations show a static flip disorder of the thiophene ring. A disorder of this kind is often observed in the case of monosubstituted thiophenes.[45] In the present case, approximately one-third of the thiophene rings are flipped (S5B−C8B). The Cr−N and Cr−C distances (average values: 2.067(3) and 2.073(4) Å) are identical with those of [CrCyclam(C≡C−Ph)$_2$]$^{+}$ [34] (2.065(4) and 2.077(3) Å), while the Ni−S and C−C distances (2.156(1) and 1.352(6) Å) are in good agreement with the values of [Ni(mdt)$_2$]$^{-}$ (2.162(2) and 1.361(10) Å).[41] The unit cell of **1** contains two [CrCyclam(C≡C−3-thiophene)$_2$][Ni(mdt)$_2$] molecules, and the crystal structure is characterized by a two-dimensional sheet of cations and anions on the *bc* plane, in which there are five short intermolecular contacts, as shown in Figure 1b. The short contacts r_1 and r_4 connect the coordinating atoms of a cation (N1, N2) and anions (S1). Because a spin distribution on the coordinating atoms is, in general, significantly higher than that on other parts of the ligand, these two contacts probably work as principal paths of intermolecular spin−spin interactions. In particular, the shorter distance of r_1 (3.575(4) Å) compared to that of r_4 (3.764(3) Å) suggests that r_1 plays the most important role in intermolecular spin−spin interactions. Despite the smaller spin density on the thiophene ring, a shorter interatomic distance of r_5 (3.459(4)) than the van der Waals distance can enhance the intermolecular exchange interaction.

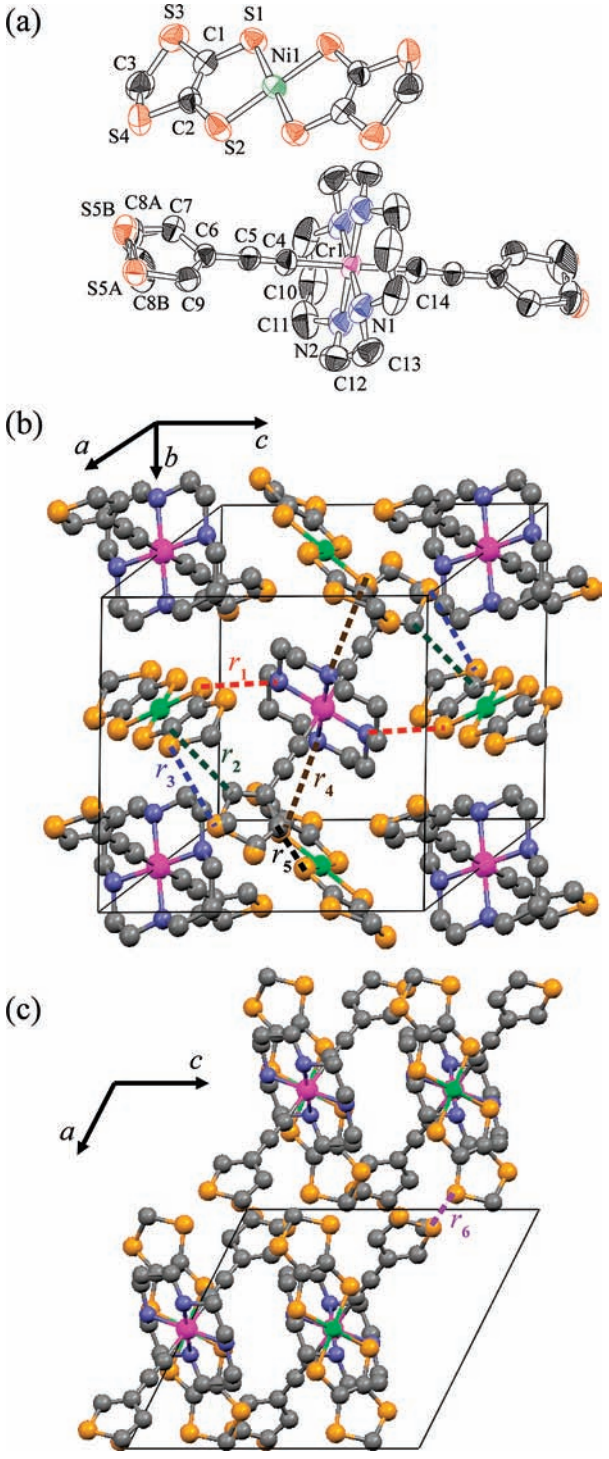

Figure 1. (a) ORTEP diagram with 50% probability level and the atom numbering scheme for **1**. (b) Two-dimensional sheet structure of **1** onto the *bc* plane. The dashed lines r_i indicate the short intermolecular contacts. r_1 (red): N1(H1)−S1, 3.575(4) Å. r_2 (green): C9−C2, 3.494(6) Å. r_3 (blue): S5A−S4, 3.795(3) Å. r_4 (brown): N2(H2)−S1, 3.764(3) Å. r_5 (black): C7−S2, 3.459(4) Å. (c) The interlayer stacking of **1** viewed along the *b* axis. Interlayer short contact r_6 (purple): S5A−S4, 3.547(3) Å.

Among the short contacts, r_3 and r_6 connect the sulfur atoms of the thiophene ring and the anion, implying that the exchange interactions through these paths are largely affected by the flip disorder of the thiophene ring.

Crystal Structure of 2. The centrosymmetric unit cell of **2** contains one [CrCyclam(C≡C−Ph)$_2$][Ni(mdt)$_2$]

(44) Burnett, M. N.; Johnson, C. K. *ORTEP-III*; Oak Ridge National Laboratory Report ORNL-6895, Oak Ridge National Laboratory: Oak Ridge, TN, **1996**.

(45) Wagner, P.; Officer D. L.; Kubicki M. *Acta Crystallogr., Sect. E* **2006**, *62*, o5745−o5747 and references therein.

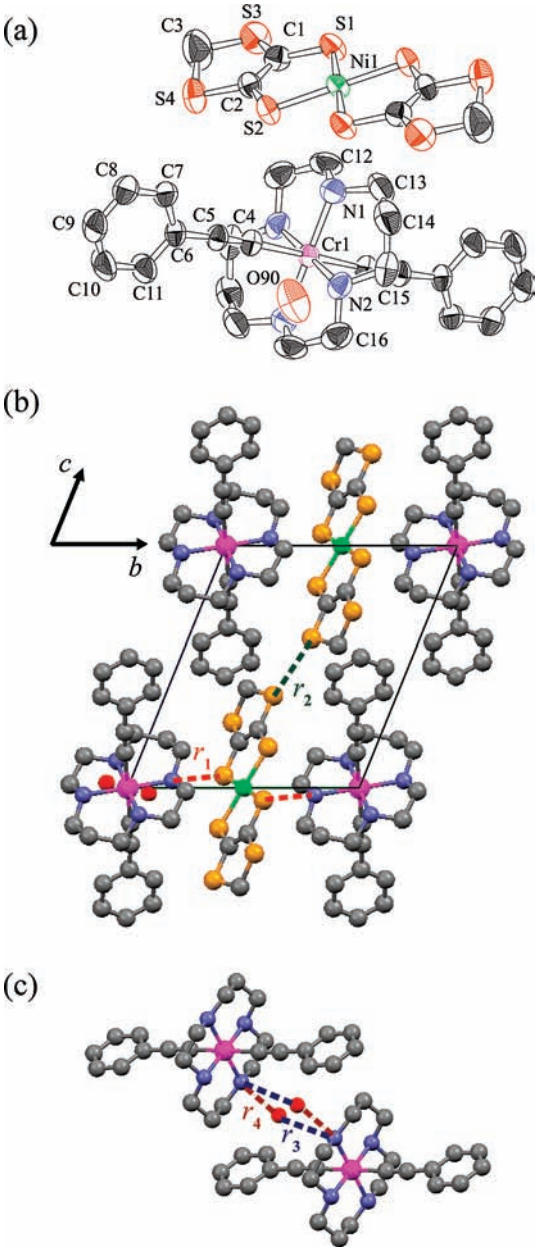

Figure 2. (a) ORTEP diagram at the 50% probability level with atom numbering scheme for **2**. (b) The crystal structure of **2**. The dashed lines r_1 and r_2 indicate the short intermolecular contacts. r_1 (red): N1(H1)−S2, 3.790(4) Å. r_2 (green): S4−S4, 3.327(2) Å. (c) The bridging water molecule between adjacent cations translated by one unit cell along the *a* axis. The water molecule occupies either of the crystallographically equivalent sites. The blue and dark red dashed lines indicate NH−O hydrogen bonds. r_3: N2H2−O90, 2.94(2) Å. r_4: N2H2−O90, 3.22(1) Å.

Table 2. Bond Lengths (Å) and Angles (deg) for **1**

Cr1−N1	2.072(3)	Cr1−N2	2.061(3)
Cr1−C4	2.073(4)	C4−C5	1.206(6)
Ni1−S1	2.170(1)	Ni1−S2	2.142(1)
C1−C2	1.352(6)	N1−Cr1−N2	84.9(1)
N1−Cr1−C4	91.2(1)	N2−Cr1−C4	87.8(1)
S1−Ni1−S2	92.30(4)		

molecule and one disordered crystal water molecule, as shown in Figure 2. The crystal shows no structural change, at least down to 100 K. The Cr−N and Cr−C distances of a cation (average values: 2.065(5), 2.073(5) Å) and Ni−S and C−C distances of an anion (average values: 2.158(2),

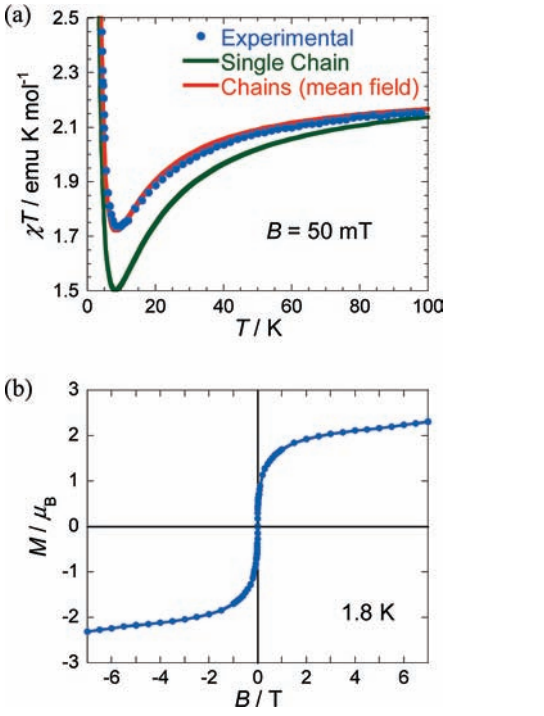

Figure 3. (a) The temperature dependence of the χT value of **1**. Solid green and red lines are the curves fitted by using eq 1 (isolated ferrimagnetic chain, intrachain interaction $2J/k_B = -7.2$ K) and eq 6 (ferrimagnetic chains with the mean field approximation, $2J/k_B = -6.1$ K and interchain interaction $2zJ'/k_B = +0.52$ K), respectively (see text). (b) The magnetization curve of **1** measured at 1.8 K.

Table 3. Bond Lengths (Å) and Angles (deg) for **2**

Cr1−N1	2.063(5)	Cr1−N2	2.067(4)
Cr1−C4	2.073(5)	C4−C5	1.207(8)
Ni1−S1	2.158(2)	Ni1−S2	2.158(2)
C1−C2	1.35(1)	N1−Cr1−N2	86.0(2)
N1−Cr1−C4	90.0(2)	N2−Cr1−C4	90.3(2)
S1−Ni1−S2	92.94(5)		

1.35(1) Å) are identical with those of **1** (Table 3). In the crystal of **2**, there are two intermolecular short contacts: r_1 between a cation and an anion and r_2 between anions. The distance between coordinating atoms S2 and N1 (3.790(4) Å) is slightly longer than that of **1**. However, in the present case, the π orbital of the S2 atom is directed to the N1 atom, bringing the enhancement of the intermolecular exchange interaction. On the other hand, though r_2 connects outside sulfur atoms having small spin densities, there is a possibility that r_2 works as an important path of exchange interaction thanks to its remarkably shorter distance (3.327(2) Å) than the van der Waals distance (3.7 Å). The water molecules in the crystal bridge cations with hydrogen bonds r_3 and r_4 along the *a* axis. Because the water molecules are enclosed by the cations and the anions, they cannot escape from the crystal even under vacuum conditions. Although the crystal of **2** is centrosymmetric as a whole, each water molecule occupies either of the neighboring crystallographically equivalent sites, resulting in the local breakdown of the inversion symmetry. This symmetry breakdown plays an important role in the magnetism, as shown later.

Magnetic Properties of 1. The temperature dependence of the χT of **1** measured under an external field of 50 mT is shown in Figure 3a, where χ is the molar magnetic

susceptibility for the nonoriented crystals after subtracting the contribution of core diamagnetism. The susceptibility roughly obeys the Curie−Weiss law in the high-temperature region with a Curie constant of 2.26 emu K mol^{-1} and a Weiss temperature of −4.3 K. The observed Curie constant is in good agreement with the sum of the spin-only values of $[CrCyclam(C{\equiv}C-3\text{-thiophene})_2]^+$ ($S = 3/2$) and $[Ni(mdt)_2]^-$ ($S = 1/2$). The χT value gradually decreases as the temperature decreases and takes a minimum of 1.73 emu K mol^{-1} at 9 K, followed by a rapid increase which reflects the ferrimagnetic nature of the material. The observed susceptibility is indeed quantitatively consistent with the model of the weakly interacted [1/2−3/2] ferrimagnetic chains shown below, where it is surmised that the spin structure of **1** can be characterized by the strong intrachain and weaker interchain interactions attributed to the short contacts r_1 and r_4, respectively. First of all, the analytical expression for the χT value of an isolated [1/2−3/2] ferrimagnetic chain is given[46] as

$$\chi_{1D}T = 0.5756\left(\frac{|2J|}{k_BT}\right)^{1.80} + 2.250\exp\left(-0.882\frac{|2J|}{k_BT}\right) \quad (1)$$

where k_B is the Boltzmann constant, and the intrachain exchange interaction J is defined in the following Hamiltonian:

$$H = -2J\sum_i S_iS_{i+1} \quad (2)$$

Then, the interchain interaction is introduced by using a simple mean field approximation:

$$\chi = \frac{\langle M\rangle}{H_{ex}} \sim \chi_{1D}(H_{ex} + H_{eff})\frac{1}{H_{ex}} \quad (3)$$

$$H_{eff} = \frac{2zJ'}{g\mu_BN}\times\frac{\langle M\rangle}{g\mu_B}(\text{mean field approximation})$$
$$= \frac{2zJ'}{g^2\mu_B^2N}\chi_{1D}(H_{ex} + H_{eff}) \quad (4)$$

$$\therefore H_{eff} = \frac{{}^{\alpha}\chi 1D}{1-{}^{\alpha}\chi 1D}H_{ex}, \alpha = \frac{2zJ'}{g^2\mu_B^2N} \quad (5)$$

$$\therefore \chi T = \chi_{1D}T\left(1+\frac{\alpha\chi_{1D}}{1-\alpha\chi_{1D}}\right) \quad (6)$$

where $\langle M\rangle$, H_{ex}, H_{eff}, zJ', g, μ_B, and N are the magnetization of a ferrimagnetic chain, the external field, the interchain interaction regarded as a mean field, the fitting parameter representing the number and the strength of the effective interchain interaction, the g value (g = 2 is used for simplicity), the Bohr magneton, and the Avogadro constant. On the basis of eqs 1 and 6, the best fit of the χT value is indistinguishable from the data, as shown in Figure 3a, with the values of the intrachain interaction $2J/k_B = -6.1$ K and interchain interaction $2zJ'/k_B = +0.52$ K. Here, it should be noted that J' does not indicate the interchain cation−anion interaction directly because J' is defined as the interaction between the "net magnetizations" of the ferrimagnetic chains. For example, the positive value of $2zJ'$ in the present case means that there is a "local" antiferromagnetic interaction between a cation and an anion in adjacent ferrimagnetic chains.

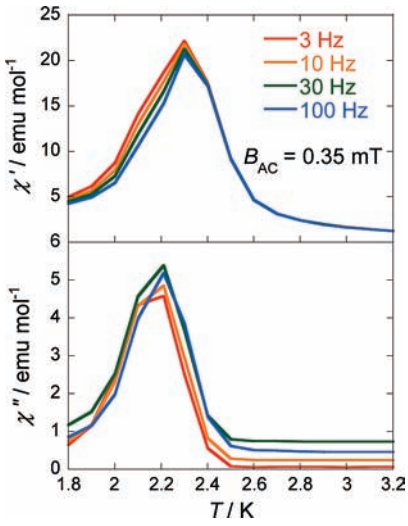

Figure 4. The temperature dependencies of χ' and χ'' of **1** measured under DC and AC fields of $B_{DC} = 0$ and $B_{AC} = 0.35$ mT.

Figure 3b shows the magnetization curve of **1** at 1.8 K. At this temperature, applying the external field substantially increases the magnetization M, and M reaches a value of 2 μ_B at around 1 T, corresponding to the ferrimagnetic [1/2−3/2] system. In the higher-field region, M exhibits a slight and almost linear increase owing to the strong intrachain antiferromagnetic interaction. Although no hysteresis loop was observed at that temperature, we can conclude that the S-shaped magnetization curve is in consequence of its ferrimagnetic ground state evidenced by the AC susceptibility, as shown in Figure 4. The in-phase (χ') and out-of-phase (χ'') susceptibilities clearly show frequency-independent peaks at around 2.3 and 2.2 K, respectively, corresponding to the magnetic phase transition of **1**. In this report, we define the transition temperature as a peak top of χ'. Despite the stronger intra- and interchain interactions of **1** than those of **2**, the transition temperature of 2.3 K is significantly lower than that of **2**, as will be shown later. The discrepancy is perhaps originated from the flip disorder of thiophene rings, which disturb the ordering.

Magnetic Properties of 2. The temperature dependence of the χT value of **2** measured under the external field of 50 mT is shown in Figure 5a. The susceptibility of **2** also approximately obeys the Curie−Weiss law in the high temperature region with the Curie constant of 2.23 emu K mol^{-1} and the Weiss temperature of −4.6 K, and the Curie constant is roughly the same as that of **1**. The χT value gradually decreases from 2.20 emu K mol^{-1} at 300 K to 1.55 emu K mol^{-1} at 6.5 K as the temperature

(46) Miller, J. S.; Drillon, M. *Magnetism: Molecules to Materials*; Wiley-VCH: Weinheim, Germany, 2001; Vol. *I*.

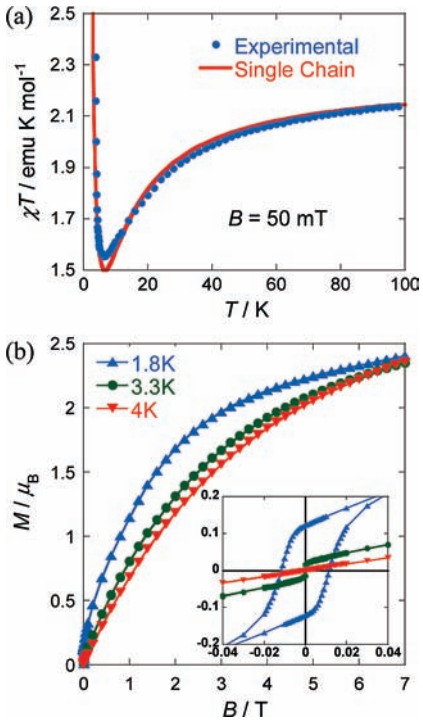

Figure 5. (a) The temperature dependence of the χT value of **2**. The solid green line is the fitted curve by using eq 1 ($2J/k_B = -5.7$ K). (b) The magnetization curves of **2** measured at 1.8, 3.3, and 4 K. The inset is the enlarged part at low field.

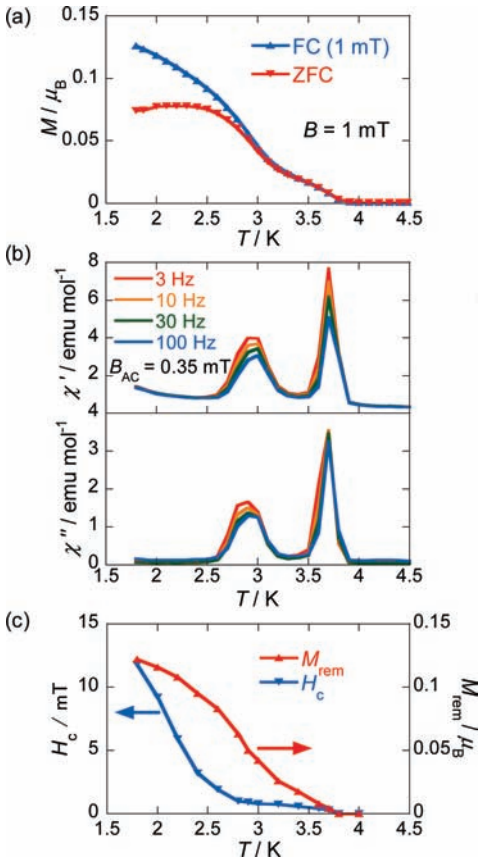

Figure 6. FC (1 mT) and ZFC magnetizations of **2** measured at 1 mT. (b) The temperature dependencies of χ' and χ'' of **2** measured under DC and AC fields of $B_{DC} = 0$ and $B_{AC} = 0.35$ mT. (c) The temperature dependencies of M_{rem} and H_c of **2**.

decreases, followed by a steep increase. In contrast with **1**, eq 1 with fitting parameter $2J/k_B = -5.7$ K is in good agreement with the experimental result at a quantitative level, indicating that the spin structure of **2** is regarded as an assembly of [1/2−3/2] ferrimagnetic chains with a strong intrachain interaction mediated by the short contact r_1, while the interchain exchange interactions through r_2, r_3, and r_4 are negligibly weak in the high-temperature region despite a remarkably short S−S distance of r_2.

The magnetization curve of **2** shows a small remnant magnetization M_{rem} below 3.7 K. Figure 5b shows the magnetization curves of **2** at three different temperatures of 1.8, 3.3, and 4 K. The magnetization curve at 1.8 K clearly shows a small hysteresis loop with $M_{rem} = 0.12\,\mu_B$ (canting angle: 3.4°) and the coercive force $H_c = 11.8$ mT. The M gradually increases and reaches a value of ca. $2\,\mu_B$ at 2.5 T, followed by a slow increasing rate above the field. The observed behavior can be explained by the weak ferromagnetism[47−57] in the weakly antiferromagnetically coupled [1/2−3/2] ferrimagnetic chains, which shows a small M_{rem} thanks to the weak ferromagnetism and faster and slower increases of the magnetization associated with weak interchain and strong intrachain antiferromagnetic interactions, respectively. We can exclude the possibility that the observed M_{rem} is originated from some ferromagnetic impurities. First, the optical microscope observation reveals that the sample consists of only quite fine needle crystals, and no other shaped material was observed. Second, the observed M_{rem} of $0.12\,\mu_B$ at 1.8 K is too large to attribute to a small amount of impurities. Third, different samples of different batches show the same value of M_{rem}. The finite M_{rem} of $0.016\,\mu_B$ observed at 3.3 K and the absence of it at 4 K indicate that the weak-ferromagnetic transition of **2** occurs between 4 and 3.3 K.

To determine the weak-ferromagnetic transition temperature, we measured the field-cooled (FC, $B = 1$ mT) and zero-field-cooled (ZFC) magnetization under a magnetic field of 1 mT. Figure 6a clearly shows a two-step phase transition. The first phase transition occurs at 3.7 K, below which the magnetization remarkably increases. The second transition is found at around 2.9 K where the FC and ZFC magnetizations become equal. The existence of the two phase transition points is obviously evidenced by the AC susceptibility shown in

(47) Dzyaloshinsky, I. *J. Phys. Chem. Solids* **1958**, *4*, 241–255.
(48) Moriya, T. *Phys. Rev.* **1960**, *120*, 91–98.
(49) Li, R.-Y.; Wang, X.-Y.; Liu, T.; Xu, H.-B.; Zhao, F.; Wang, Z.-M.; Gao, S. *Inorg. Chem.* **2008**, *47*, 8134–8142.
(50) Gao, E.-Q.; Yue, Y.-F.; Bai, S.-Q.; He, Z.; Yan, C.-H. *J. Am. Chem. Soc.* **2004**, *126*, 1419–1429.
(51) Moriya, T. *Phys. Rev.* **1960**, *117*, 635–647.
(52) Setifi, F.; Golhen, S.; Ouahab, L.; Miyazaki, A.; Okabe, K.; Enoki, T.; Toita, T.; Yamada, J. *Inorg. Chem.* **2002**, *41*, 3786–3790.
(53) Wang, Z.; Zhang, B.; Inoue, K.; Fujiwara, H.; Otsuka, T.; Kobayashi, H.; Kurmoo, M. *Inorg. Chem.* **2007**, *46*, 437–445.
(54) Wang, X.-Y.; Wang, Z.-M.; Gao, S. *Inorg. Chem.* **2008**, *47*, 5720–5726.
(55) Feyerherm, R.; Loose, A.; Ishida, T.; Nogami, T.; Kreitlow, D. B.; Litterst, F. J.; Süllow, S.; Klauss, H.-H.; Doll, K. *Phys. Rev. B* **2004**, *69*, 134427_1−8.
(56) Setifi, F.; Ouahab, L.; Golhen, S.; Miyazaki, A.; Enoki, T.; Yamada, J. *C. R. Chim.* **2003**, *6*, 309–316.
(57) Turner, S. S.; Pevelen, D. L.; Day, P.; Prout, K. *J. Chem. Soc., Dalton Trans.* **2000**, 2739–2744.

Figure 6b, in which there are two frequency-independent peaks at around 2.9 and 3.7 K, indicating the magnetic phase transitions at those temperatures. Here, it should be noted that the existence of the two phase transition points cannot be attributed to the coexistence of two kinds of materials (or two kinds of ground states) having higher and lower transition temperature. As shown later, the material shows a small H_c in the temperature range of $3.7 > T > 2.9$ K and a large H_c at $T < 2.9$ K. If the sample consists of two kinds of materials having a high transition temperature−lower H_c and a low transition temperature−higher H_c, the magnetization curve at 1.8 K must show two anomalies corresponding to lower and higher H_c's. Therefore, the absence of an anomaly in the low field region of the magnetization curve of **2** at 1.8 K strongly suggests that the two-step phase transition is an intrinsic characteristic of **2**. Judging from the magnetization curves shown in Figure 5b and the low-field magnetizations shown in Figure 6a, we can conclude that the first phase transition at 3.7 K is an ordinary weak-ferromagnetic transition. In the temperature range $3.7 > T > 2.9$ K, the M_{rem} increases monotonically from 0.004 to 0.051 as the temperature decreases, while a slow approach of the H_c to 0.8 mT was observed, as shown in Figure 6c. On the other hand, the H_c increases markedly below the second phase transition temperature of 2.9 K, while M_{rem} increases continuously as the temperature decreases. Although the detail and the mechanism of the second phase transition remain unclear, the transition drastically enhances the magnetic anisotropy of **2**.

Generally, there are two candidates for the origin of spin canting, that is, antisymmetric exchange interaction (Dzyaloshinsky−Moriya (DM) interaction) and single-ion anisotropy.[47−56] In the present case, the contribution of the single-ion anisotropy can be excluded because the unit cell of **2** contains only a cation (anion) molecule, where the anisotropy axes of all cations (anions) are oriented along the same direction and have no contribution to the weak ferromagnetism. On the other hand, in the centrosymmetric unit cell of **2**, the local symmetry breakdown caused by water molecules allows a DM interaction between adjacent cations, resulting in the observed weak ferromagnetism.

Summary

New molecule-based magnets [CrCyclam(C≡C−3-thiophene)$_2$][Ni(mdt)$_2$] (**1**) and [CrCyclam(C≡C−Ph)$_2$][Ni(mdt)$_2$]-(H_2O) (**2**) were prepared and structurally and magnetically investigated. The crystal **1** is characterized by ferrimagnetic chains of cations and anions with an intrachain exchange interaction $2J/k_B = -6.1$ K. The interchain effective ferromagnetic interaction $2J'/k_B = +0.52$ makes **1** two-dimensional and brings a ferrimagnetic transition at 2.3 K with $H_c < 0.5$ mT. The crystal structure of **2** also consists of ferrimagnetic chains with intrachain interaction $2J/k_B = -5.7$ K. Though the interchain interaction of **2** intermediated by a water molecule is negligibly weak in the high-temperature region, the interaction leads to the weak-ferromagnetic transition at 3.7 K. Below that temperature, M_{rem} gradually increases as the temperature decreases, while H_c maintains a value smaller than 1 mT. Although the origin and the mechanism are as yet obscure, the second magnetic phase transition occurs at 2.9 K accompanied by a steep increase of H_c below that temperature, while M_{rem} increases monotonically. The origin of the weak ferromagnetism can be explained by the DM interaction brought by a water molecule which occupies either of the neighboring crystallographically equivalent sites attendant with the local symmetry breakdown.

Acknowledgment. This work was supported by a Grant-in-Aid for Scientific Research No. 20750119 from the Ministry of Education, Culture, Sports, Science and Technology, Japan.

Supporting Information Available: X-ray crystallographic data in CIF format are available free of charge via the Internet at http://pubs.acs.org.